Alloys

DOI: 10.1002/ange.201207491

A Strategy for Designing a Concave Pt–Ni Alloy through Controllable Chemical Etching**

*Yuen Wu, Dingsheng Wang, Zhiqiang Niu, Pengcheng Chen, Gang Zhou, and Yadong Li**

During the past few decades, substantial advances in the so-called "bottom-up" synthesis has allowed the precise incorporation of atoms into semiconductor[1] or metallic[2] nanoparticles (NPs), that have well-defined structures and fascinating properties. Moreover, with stepwise bottom-up strategy, it is possible to open up the synthetic route to produce core–shell,[3] branched,[4] alloy,[5] and hybrid[6] structures. Combining the "bottom-up" strategy and a subsequent "top-down" carving process, a class of Au–Ag hollow and framework structures has been synthesized through galvanic replacement method.[7] Based on this train of thought, polymetallic hollow NPs with higher complexity could be produced by a sequential galvanic exchange and a Kirkendall growth method.[8] These metal nanostructures with characteristic high surface area and hollow interior have had great success in optical sensing,[9] catalysis,[10] and drug delivery.[11]

Through selectively etching away the less-noble metal and the subsequent rearrangement the remaining metal atoms, the chemical etching approach has been shown to be an effective and classical "top-down" method to simultaneously control shape, size, and composition of metallic nanostructures.[12] In 1926, the industrial catalyst Raney nickel was developed by selectively removing most of the aluminum from an Ni–Al alloy.[13] This "old" material with a porous structure is used as an important catalyst for the hydrogenation of vegetable oils to this day. Inspired by this approach, our group has recently synthesized a nanoporous Pt–Ni alloy which has enhanced catalytic activity.[14] However, chemical etching suffers from some intrinsic drawbacks, including that the surface atoms of alloy are usually etched in random sites[15] and the etching process is usually too drastic to control.[16] Improving the chemical etching technique by making it moderate and controllable is still a great challenge. We predict that, manipulating both the "bottom-up" and "top-down" processes at nanoscale could enrich the family of bimetallic structures.

We use coordinating complexes to control the chemical etching process at room temperature to synthesize a concave structure. In a typical procedure, 4 mg octahedron shaped Pt–Ni alloy particles were dispersed in 1 mL water, and an excess of dimethylglyoxime (10 mg dissolved in 1 mL ethanol). After stirring for 12 h, dilute acetic acid (50%) was added to dissolve the nickel dimethylglyoxime generated. The concave Pt–Ni alloy particles were obtained after washing and centrifugation. To further understand the nature of the controllable etching process, we also carried out theoretical investigations using density functional theory (DFT) calculations to support experimental observations. Indeed, the atomic cohesive energy (E_{coh}) regarding the chemical potentials of species in the alloys was identified as governing the different etching priorities on specific sites during the etching process, determining the structure obtained. Remarkably, owing to larger surface area and higher density of exposed atomic steps,[17] the concave nanostructures exhibited superior activity over the octahedral Pt–Ni alloy particles for both the electro-oxidation of methanol and hydrogenation of nitroarenes.

Figure 1a showed transmission electron microscope (TEM) image of the starlike corroded $PtNi_2$ NPs which have six uniform arms. Most of the particles lie flat on the

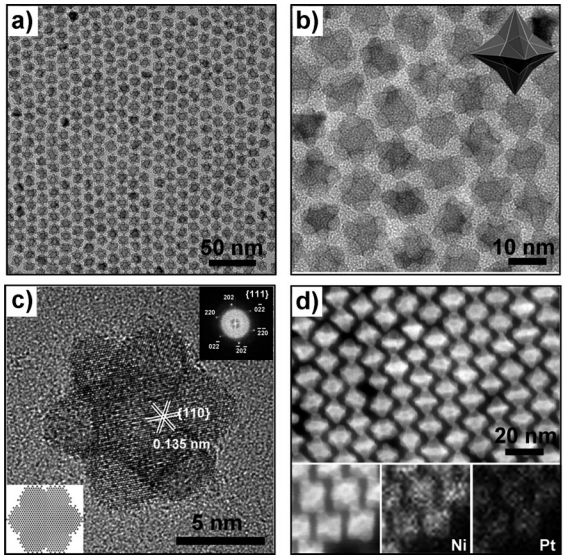

Figure 1. a) TEM image and b) magnified TEM image of corroded $PtNi_2$. Inset is the ideal model of a concave octahedron. c) HRTEM image of corroded $PtNi_2$ orientated along {111} direction. Insets are the FFT (fast Fourier transition) patterns and corresponding lattice ball models. d) HAADF-STEM image and corresponding elemental maps (Pt and Ni) of corroded $PtNi_2$ particles.

[*] Y. E. Wu, D. S. Wang, Z. Q. Niu, Prof. Y. D. Li
Department of Chemistry
Tsinghua University, Beijing 100084 (China)
E-mail: ydli@mail.tsinghua.edu.cn
P. C. Chen, G. Zhou
Department of Physics
Tsinghua University, Beijing 100084 (China)

[**] This work was supported by the State Key Project of Fundamental Research for Nanoscience and Nanotechnology (2011CB932401 and 2011CBA00500), the National Natural Science Foundation of China (Grant No. 20921001 and 21131004).

Supporting information for this article is available on the WWW under http://dx.doi.org/10.1002/anie.201207491.

substrate using three adjacent arms. As shown in magnified TEM image and the high-angle annular dark-field scanning transmission electron microscope (HAADF-STEM) micrograph (Figure 1 b,c, and d), the six arms were much brighter than the center region of the particles and each face of NPs was excavated resulting in a curved cavity, indicating the presence of the concave structure. The corresponding elemental maps of HAADF-STEM micrograph showed that both Pt and Ni were distributed evenly throughout each individual concave nanocrystal. The high-resolution TEM (HRTEM) images of a single concave Pt–Ni NP from different directions (Figure 1 c and Figure S1 of Supporting information) clearly showed the surface contained rich steps and defects. Previous synthesis have allowed us to prepare a series of octahedral Pt–Ni nanocrystals (average size: 11.8 nm) which were strictly bounded by six {111} facets.[18] The octahedral Pt–Ni NPs have excellent monodispersity and were coated with hydrophilic surfactant molecules allowing them to be dispersed in various polar solvents, benefiting the interaction with the water-soluble ligand (dimethylglyoxime) in the subsequent chemical etching procedure (Figure S2 of the Supporting Information).

Figure 2 shows TEM and HRTEM images of Pt–Ni NPs prepared with increasing concentrations of Ni (Ni:Pt mole ratio was varied from 2:1 to 3:1 and 10:1). Since more and more Ni could be dissolved from Ni-rich Pt–Ni alloy, the concavity of the obtained nanocrystals significantly increased as the nickel content of the starting alloys increased. Powder X-ray diffraction (XRD) measurements of Pt–Ni NPs were used to identify the internal crystalline structures (Figure S4). The diffraction patterns of the Pt–Ni alloys could be indexed to {111}, {200}, and {220} diffractions of a face-centered-cubic (fcc) structure. After chemical etching, all the peaks of the corroded Pt–Ni alloys shifted slightly to a lower 2θ value compared to those of uncorroded Pt–Ni alloys, which could be attributed to the increased lattice spacing resulting from most of Ni being etched from the Ni-rich precursors. Intriguingly the XRD results suggested that all the initially Ni-rich Pt–Ni alloys gradually eroded into concave structures, all with the composition Pt_3Ni. The accurate compositions were further verified by energy dispersive spectroscopy (EDS) and inductively coupled plasma-mass spectrometry (ICP-MS) (Figure S5 and Table S1)

In the synthesis of the concave Pt–Ni bimetallic nanostructure, the dimethylglyoxime played a crucial role. The chemical etching process can be described by the chemical equilibrium Equations (1)–(3).

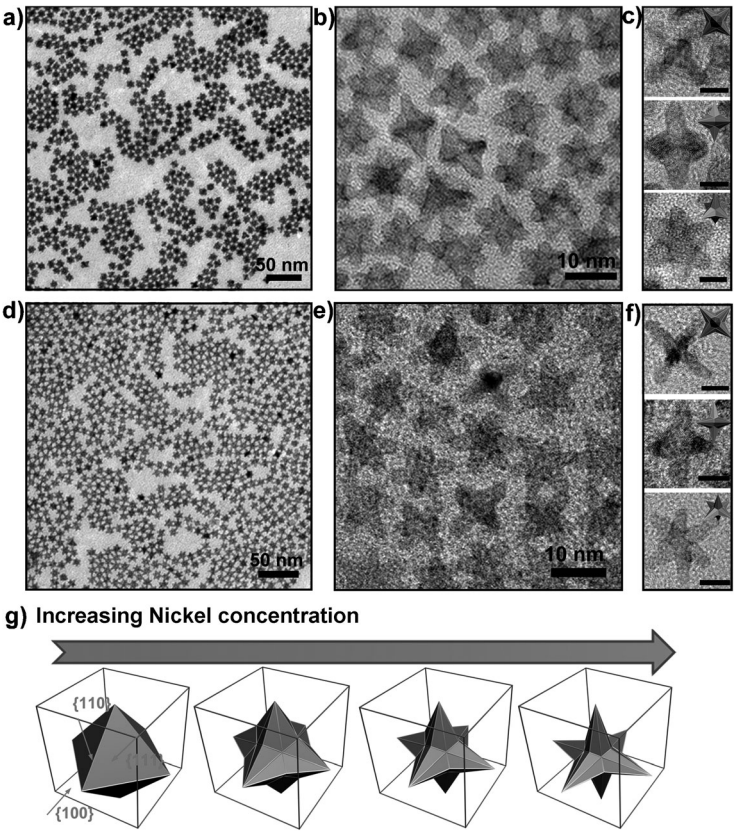

Figure 2. TEM images of a) corroded $PtNi_3$ and d) corroded $PtNi_{10}$. Magnified TEM images of b) corroded $PtNi_3$ and e) corroded $PtNi_{10}$. c) and f) are the HRTEM images and corresponding models orientated along {100} (top panel), {110} (middle panel), and {111} (bottom panel) directions, respectively (scale bars are 5 nm). g) The evolution of nanoparticle shape as a function of Ni:Pt mole ratio in the originally Ni-rich alloys.

$$Ni^0 - 2e^- \rightleftharpoons Ni^{II} \quad (1)$$

$$1/2\,O_2 + H_2O + 2\,e^- \rightleftharpoons 2OH^- \quad (2)$$

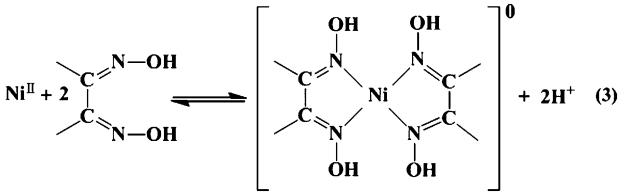

(3)

The Equations (1) and (2) could be considered as two half-reactions of an oxidation–reduction reaction. The typical synthetic procedure is shown in Figure S6, initially, the Ni atoms on the surface were oxidized to Ni^{II} by the oxygen in the air. To test this hypothesis, an experiment showed the rate of the etching process could be enhanced by the presence of oxygen. When the oxygen was replaced with the nitrogen, the etching process barely occurred (Figure S7). For Equation (3), the dimethylglyoxime selectively coordinates to Ni^{II} rather than Pt^{II} to generate a red dimethylglyoxime nickel precipitate under neutral conditions, indicating the higher susceptibility and dissolution rate of Ni species compared to Pt.[19] Quite strikingly, Pt species were not detected by ICP-MS measurements of the mother solution after washing and separation, implying Pt was not be etched from the staring polyhedrons. This result strongly supports the above view about the chemical etching process. Finally, dilute acetic acid

(50 %) could be added to dissolve the as-produced precipitate according to the Equation (3), which could be traced and verified by the X-ray photoelectron spectroscopy (XPS) experiments (see Figure S8). Surprisingly, the chemical etching process did not occur without assistance of dimethylglyoxime even at an elevated temperature (100 °C). However, the dimethylglyoxime could not completely etch all the Ni atoms from Pt–Ni alloys, even if the reaction time was lengthened or the dosage of dimethylglyoxime was increased. These interesting phenomena could be understood by carrying out measurements on redox potentials of Pt–Ni NP decorated electrode. (Figure S9) The oxidation potentials (vs. Ag/AgCl) of a Pt–Ni NP decorated electrode decreased when the Ni concentration increased or dimethylglyoxime was introduced, indicating the metal atoms could lose electrons and then dissolve from NPs much easier. Further, in our control experiment, the octahedral Pt_3Ni could not be etched by dimethylglyoxime, which means that the Pt_3Ni was a stable phase in this chemical environment. As the chemical etching proceed, the oxidation potential of the Ni-rich alloy increased with the increasing ratio of Pt to Ni, revealing that as the alloy corroded it became more difficult to be etched and finally terminated in Pt_3Ni.

The controllability of this chemical etching method was shown to be essential for the formation of this metastable concave structure. We used octahedral $PtNi_{10}$ as a probe to gain insight into the morphological evolution during the etching process. Figure 3 shows a series of NPs with an increasing concavity could be obtained during different stages of chemical etching. In the initial stage, the etching process prevailed along the {100} direction and change the octahedrons into round particles, which suggested the etching process started at the corners first. When the new narrow {100} facets formed, the etching shifted to the {110} and {111} directions. In a further step of the etching process, the edges and the facets would be excavated to curved cavities and then the concave structure is generated. However, the severely corrosive conditions, such as concentrated nitric acid treatment usually detach the surface ligands and distort this metastable nanostructure, resulting in aggregation of the NPs and collapse of concave structure (Figure S10 of SI).

Chemical etching reflects, to a certain extent, the stability of the metal atoms of NPs in the reaction environment, which could be correctly described by the E_{coh} of alloys (see Supporting Information for details). As shown in Table S3, the value of E_{coh} not only varied with the nature of metal (Ni or Pt) but also with the geometrical site (corner (C), edge (E), or face (F)). From the thermodynamic point of view, the calculated E_{coh} showed the possibility of removal of metal atoms from a $PtNi_3$ octahedron decreased in the order of $C_{Ni} > E_{Ni(Ni)} > E_{Ni(Ni\text{-}Pt)} > C_{Pt} > F_{Ni} > E_{Pt(Ni\text{-}Pt)} > F_{Pt}$ in the same reaction environment. The schematic illustration of the proposed etching process of $PtNi_3$ NPs based on DFT calculations and structural dynamics analysis are summarized in Figure 4. More precisely, for the corners and edges, the Ni atoms were preferably removed, followed by the deposition and segregation of the remaining Pt atoms (Figure 4 b and c), forming round corners and steps. This result was in agreement with the HRTEM observations in Figure 3. While for the (111) surface of the octahedron, the Ni atoms were present in much greater numbers than the Pt atoms, so the dissolution rate of the Ni atoms was much more pronounced than the diffusion-segregation rate of the Pt atoms (Figure 4 d), indicating the predominant role of exfoliation etching. Furthermore, for the same kind of atoms, the faces are more stable sites than the corners and edges because of the E_{coh} of the faces is higher than those of the corners and edges (Table S3). Thus, the etching started from corner sites rather than {111} faces. The proposed etching process and the increasing Pt/Ni ratio of corroded NPs were in agreement with the experimental observations (detailed discussion in Supporting Information) Noted that only Pt-segregation occurs in corroded NPs because the Ni atoms were dissolved in the solution, which was quite different from the cases of Pt_3Ni single-crystals.[20] DFT calculations also showed that the density of states (DOS) at (and near) the Fermi level of the corroded surfaces was more than twice (and four times) those of {111} surface of Pt_3Ni single-crystal (Figure S11), indicating that concave Pt_3Ni NPs had a higher activity than single-crystal ones. Another type of Pt–Ni alloy with a predictable concave cubic morphology was also obtained by our method, if the original octahedron was replaced with a $PtNi_3$ cube. The TEM and HRTEM images of concave cubic Pt_3Ni were shown in Figure S12.

Brunauer–Emmett–Teller (BET) measurements were used to analyze

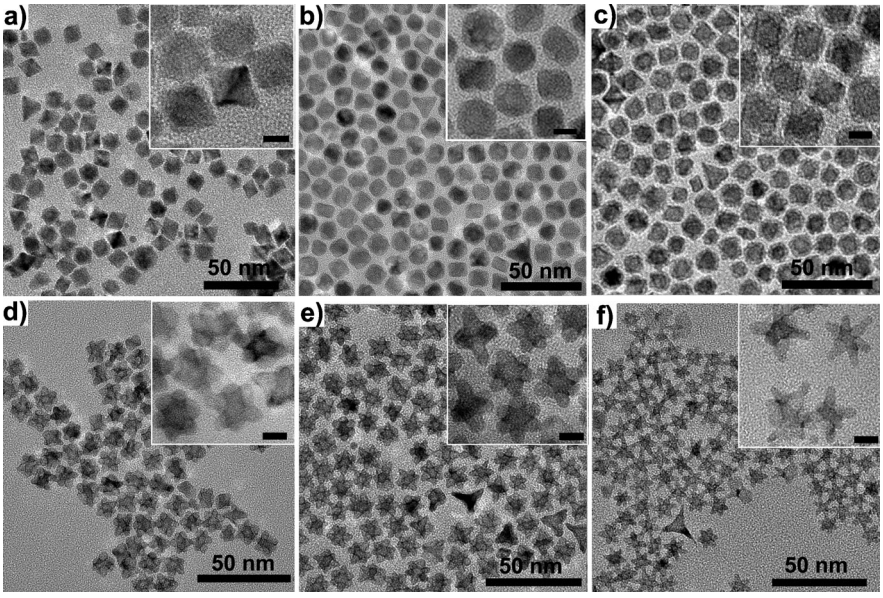

Figure 3. Shape evolution of octahedral $PtNi_{10}$ at different chemical etching stage a) 15 min, b) 30 min, c) 1 h, d) 3 h, e) 6 h, f) 12 h. Insets are the corresponding HRTEM images (scale bars are 5 nm).

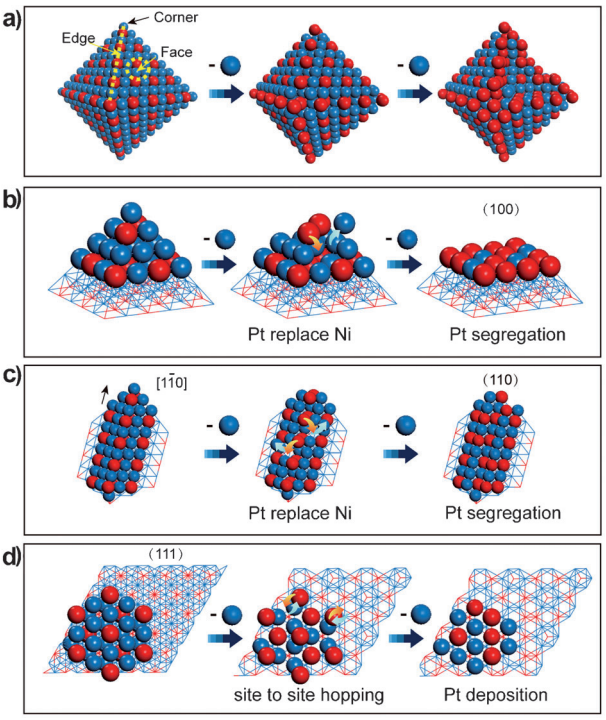

Figure 4. Schematic illustration of the proposed etching mechanism of $PtNi_3$ from DFT calculations, combined with a structural dynamics analysis. a), b), c), and d) show the evolution of whole nanoparticles, a Ni corner, a {110} edge, and a {100} face, respectively. Red and blue balls correspond to Pt and Ni atoms. Deposition of Pt atoms and removal of Ni atoms are indicated by orange and blue arrows, respectively.

the surface area of octahedral Pt–Ni NPs and corroded Pt–Ni alloys (Figure S13). The chemical etching treatment gave the corroded $PtNi_3$ ($64\ m^2 g^{-1}$) a larger surface area than the octahedral $PtNi_3$ ($38\ m^2 g^{-1}$).

To test catalytic properties, the cyclic voltammetry (CV) and electrocatalytic oxidation of methanol were used to evaluate the electrochemical activity of as-synthesized Pt–Ni alloys. Measuring the charge collected in the electrochemical absorption/desorption region of 0–0.40 V and assuming a value of $210\ \mu C\,cm^{-2}$ for the adsorption of a monolayer of hydrogen on platinum, the corroded $PtNi_{10}$ showed the highest specific electrochemically active surface area (ECSA) ($71.5\ m^2 g_{Pt}^{-1}$) compared with the other corroded $PtNi_3$ ($67.5\ m^2 g_{Pt}^{-1}$) and corroded $PtNi_2$ ($52.3\ m^2 g_{Pt}^{-1}$), results which correlate with the degree of concavity (Figure 5a). Figure 5b and 5c show the corroded $PtNi_3$ was much more active and durable in the methanol oxidation. As summarized in Table S2, the peak current densities of methanol oxidation in the forward (positive) potential (J_f) were: corroded $PtNi_3$ > corroded $PtNi_2$ > corroded $PtNi_{10}$ which were, respectively, around 2.4, 3.2, and 3.8 times higher than for the uncorroded NPs. Furthermore, the specific activity of corroded $PtNi_3$ was still at 73% of the original value after the durable test, which was higher than for the octahedral $PtNi_3$ and Pt_3Ni (Figure 5c). Methanol can be oxidized to CO species which poison the Pt catalyst sites and limit their activity.[21] Atomic steps on Pt offer a superior activity for the oxidation of CO,[22] thus the improved activity of methanol oxidation on corroded Pt–Ni alloys could be attributed to the high density of Pt-segregated atomic steps. To confirm that the corroded Pt–Ni alloys have a better tolerance to poisoning CO, CO stripping experiments were conducted. As shown in Figure S16, the peak potentials of corroded Pt–Ni alloys were more negative than for Pt–Ni octahedrons, showing the enhanced CO-removal ability of the corroded P-t-Ni alloys.

The structure of the concave Pt–Ni alloy also suggested potential as a heterogeneous catalyst. We chose the corroded $PtNi_3$, octahedral Pt_3Ni, and $PtNi_3$ as probes to study the structure–activity dependences in the hydrogenation reactions of nitroarenes, which are important industrial process.[23] Catalysis by corroded $PtNi_3$, Figure 5d showed the nitrobenzene was completely converted with nearly 100% selectivity in 3 h. As listed in Table S4, the calculated initial activities turnover frequency (TOF) of corroded $PtNi_3$ was 7.9, and 10.5-times higher than that catalyzed by octahedral $PtNi_3$ and Pt_3Ni. Further, the catalyst with concave structure had enhanced catalytic activity in various hydrogenations of nitroarenes under similar conditions.

In summary, this work presents a controllable "top-down" synthesis of concave Pt–Ni alloys through a coordination-assisted chemical-etching process. Based on the experimental observations and DFT calculations, the formation of the concave structure was attributed to the different etching priorities on specific sites. Owing to the larger surface area and higher density of exposed atomic steps, concave Pt–Ni alloys exhibited higher catalytic activity compared to the uncorroded precursors. We foresee that our method would open the way to design special morphologies and structures of bimetallic nanocrystals, which could find use in various applications.

Experimental Section

Chemical etching treatment of Pt–Ni alloy: The as-prepared Pt–Ni (4 mg) alloy was dispersed in H_2O (1 mL) and dimethylglyoxime (10 mg dissolved in 1 mL ethanol) added. The reaction mixture was stirred for 12 h. Acetic acid (5 mL; 50%) was added and stirred for a further 15 min. The products were collected by centrifugation and further washed by ethanol for three times.

Characterization: The crystalline structure and phase purity were determined by Rigaku RU-200b X-ray powder diffractometer with CuKa radiation ($l = 1.5418$ Å). The composition of the product was measured by the inductively coupled plasma-mass spectrometry (ICP-MS) and energy dispersive spectrometer (EDS). TEM images were recorded by a JEOL JEM-1200EX working at 100 kV. HRTEM images were recorded by a FEI Tecnai G2 F20 S-Twin high-resolution transmission electron microscope working at 200 kV and a FEI Titan 80–300 transmission electron microscope equipped with a spherical aberration (Cs) corrector for the objective lens working at 300 kV. X-ray photoelectron spectroscopy (XPS) experiments were performed on a ULVAC PHI Quantera microprobe. Binding energies (BE) were calibrated by setting the measured BE of C 1s to 284.8 eV. Brunauer-Emmett-Teller (BET) surface area was measured with N_2 at 77 K by using a Quantachrome Autosorb-1 instrument. Electrochemical measurements were conducted on CH Instrument 660D electrochemical analyzer. The catalytic reaction results were measured by gas chromatography (GC) (SP-6890) and ^{1}H NMR spectroscopy. The

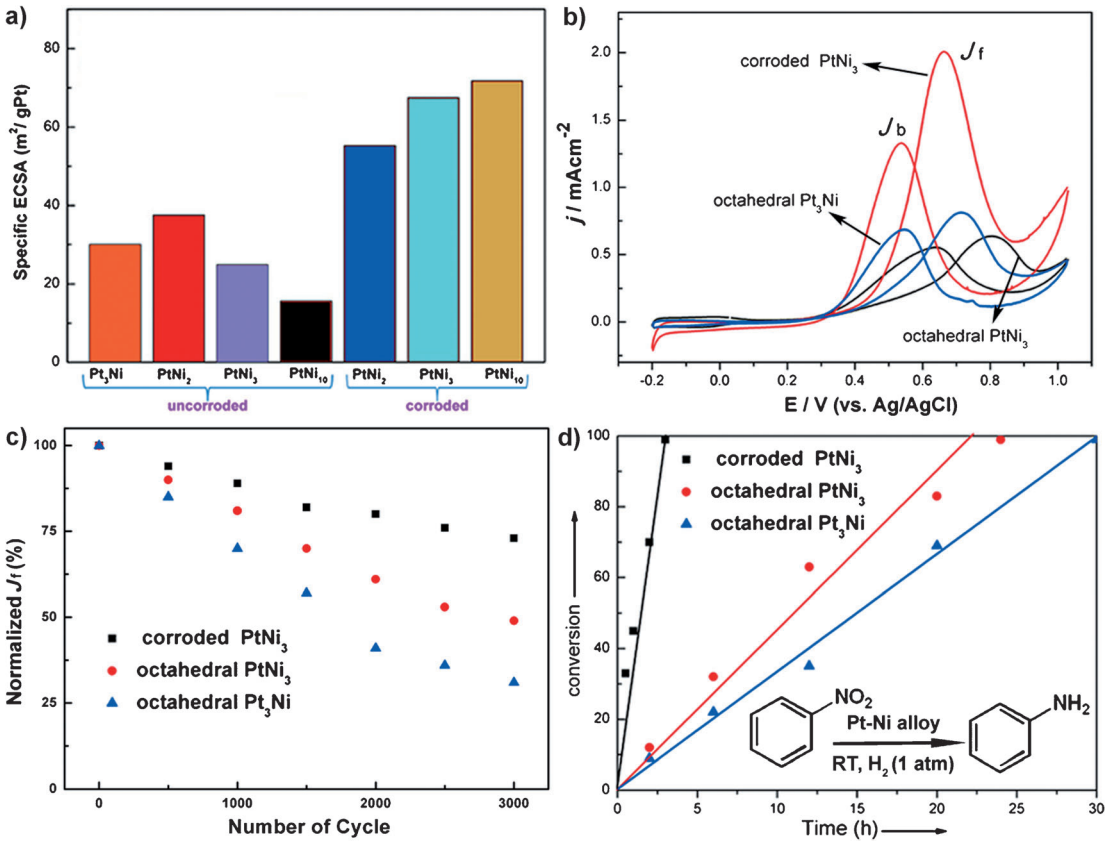

Figure 5. a) specific ECSAs for Pt–Ni alloys recorded in 0.1 M $HClO_4$ and b) cyclic voltammograms of methanol oxidation on Pt–Ni octahedrons and corroded Pt–Ni alloys in 0.1 M $HClO_4$ containing 1 M MeOH (f = forward scan, b = backward scan). c) Loss of peak current density in a forward scan as a function of cycling numbers. d) Conversion % as a function of time in hydrogenation of nitrobenzene catalyzed by octahedral $PtNi_3$, octahedral Pt_3Ni, and corroded $PtNi_3$ nanocrystals.

NMR spectroscopy was conducted on a JEOL JNM-ECX 400 MHz instrument.

Received: September 16, 2012
Published online: November 6, 2012

Keywords: nanoparticles · concave structure · etching · nickel · step atoms

[1] a) C. Murray, D. Norris, M. G. Bawendi, *J. Am. Chem. Soc.* **1993**, *115*, 8706; b) X. Peng, L. Manna, W. Yang, J. Wickham, E. Scher, A. Kadavanich, A. Alivisatos, *Nature* **2000**, *404*, 59.
[2] a) S. Sun, C. Murray, D. Weller, L. Folks, A. Moser, *Science* **2000**, *287*, 1989; b) X. Wang, J. Zhuang, Q. Peng, Y. Li, *Nature* **2005**, *437*, 121; c) Y. Sun, Y. Xia, *Science* **2002**, *298*, 2176.
[3] S. E. Habas, H. Lee, V. Radmilovic, G. A. Somorjai, P. Yang, *Nat. Mater.* **2007**, *6*, 692.
[4] B. Lim, M. Jiang, P. H. C. Camargo, E. C. Cho, J. Tao, X. Lu, Y. Zhu, Y. Xia, *Science* **2009**, *324*, 1302.
[5] A. K. Sra, R. E. Schaak, *J. Am. Chem. Soc.* **2004**, *126*, 6667.
[6] J. E. Macdonald, M. B. Sadan, L. Houben, I. Popov, U. Banin, *Nat. Mater.* **2010**, *9*, 810.
[7] Y. Sun, B. T. Mayers, Y. Xia, *Nano Lett.* **2002**, *2*, 481.
[8] E. González, J. Arbiol, V. F. Puntes, *Science* **2011**, *334*, 1377.
[9] M. J. Mulvihill, X. Y. Ling, J. Henzie, P. Yang, *J. Am. Chem. Soc.* **2010**, *132*, 268.
[10] J. Biener, A. Wittstock, L. Zepeda-Ruiz, M. Biener, V. Zielasek, D. Kramer, R. Viswanath, J. Weissmüller, M. Bäumer, A. Hamza, *Nat. Mater.* **2009**, *8*, 47.
[11] M. S. Yavuz, Y. Cheng, J. Chen, C. M. Cobley, Q. Zhang, M. Rycenga, J. Xie, C. Kim, K. H. Song, A. G. Schwartz, *Nat. Mater.* **2009**, *8*, 935.
[12] a) A. Wittstock, V. Zielasek, J. Biener, C. Friend, M. Bäumer, *Science* **2010**, *327*, 319; b) M. J. Mulvihill, X. Y. Ling, J. Henzie, P. Yang, *J. Am. Chem. Soc.* **2010**, *132*, 268.
[13] M. Raney, US patent **1926**, 1628190.
[14] D. Wang, P. Zhao, Y. Li, *Sci. Rep.* **2011**, *1*, 37.
[15] a) K. Sieradzki, J. Erlebacher, A. Karma, N. Dimitrov, M. Aziz, *Nature* **2001**, *410*, 450; b) J. I. Shui, C. Chen, J. C. M. Li, *Adv. Funct. Mater.* **2011**, *21*, 3357.
[16] G. Blonder, *Phys. Rev. B* **1986**, *33*, 6157.
[17] a) X. Q. Huang, Z. P. Zhao, J. M. Fan, Y. M. Tan, N. F. Zheng, *J. Am. Chem. Soc.* **2011**, *133*, 4718; b) Z. Niu, D. Wang, R. Yu, Q. Peng, Y. Li, *Chem. Sci.* **2012**, *3*, 1925.
[18] Y. Wu, S. Cai, D. Wang, W. He, Y. Li, *J. Am. Chem. Soc.* **2012**, *134*, 8975.
[19] D. B. Gazda, J. S. Fritz, M. D. Porter, *Anal. Chim. Acta* **2004**, *508*, 53.
[20] V. R. Stamenkovic, B. Fowler, B. S. Mun, G. Wang, P. N. Ross, C. A. Lucas, N. M. Marković, *Science* **2007**, *315*, 493.
[21] S. Wasmus, A. Küver, *J. Electroanal. Chem.* **1999**, *461*, 14.
[22] Q. S. Chen, F. J. Vidal-Iglesias, J. Solla-Gullón, S. G. Sun, J. M. Feliu, *Chem. Sci.* **2012**, *3*, 136.
[23] H. U. Blaser, H. Steiner, M. Studer, *ChemCatchem* **2009**, *1*, 210.